Title
Investigation of virus crystal growth mechanisms by in situ atomic force microscopy.

Journal
Physical review letters, 75(14)

ISSN
0031-9007

Authors
Malkin, AJ
Land, TA
Kuznetsov, YG
et al.

Publication Date
1995-10-01

DOI
10.1103/physrevlett.75.2778

Investigation of Virus Crystal Growth Mechanisms by *In Situ* Atomic Force Microscopy

A. J. Malkin,[1] T. A. Land,[2] Yu. G. Kuznetsov,[1] A. McPherson,[1] and J. J. DeYoreo[2]

[1]*Department of Biochemistry, University of California, Riverside, California 92521*

[2]*Department of Chemistry and Material Science, Lawrence Livermore National Laboratory, Livermore, California 94550*

(Received 19 May 1995)

For the first time, virus crystal growth dynamics and morphology have been investigated in real time on the nanometer scale. Individual monomers on the (111) face of cubic satellite tobacco mosaic virus (STMV) crystals were resolved and used to determine crystal packing. Growth of STMV proceeded by two- and three-dimensional nucleation to formed "stacks" of islands. No dislocations were observed. Small islands provided an estimate of critical radius size and the free energy of the step edge, α. Step advancement rates were used to determinate the kinetic coefficient β. Images illustrate mechanisms for defect incorporation and suggest factors that limit growth rate and uniformity.

PACS numbers: 87.15.Da, 61.16.Ch, 61.50.Cj, 68.35.Bs

Controlled crystallization of biological macromolecules such as proteins and viruses is central to the determination of macromolecular structure [1,2]. However, crystallization of macromolecules is highly problematic, in large part because little is known of the growth mechanisms, fundamental thermodynamic and kinetic parameters, the role of transport processes, mechanisms of defect incorporation, or the forces responsible for the orientation and bonding of the molecules in the lattice. In contrast, significant advances in our understanding of inorganic crystallization have resulted from extensive studies of inorganic, single crystal surfaces. One of the major results to emerge from scanned probe microscopy investigations of epitaxial growth of semiconductor surfaces is that the surface morphology is determined primarily by the kinetics of atomic motion on terraces and not by the equilibrium thermodynamics of step configuration [3,4,5]. Not only do these kinetic effects determine the distribution and size of islands [3] as well as the rate at which atoms are added to preexisting steps, but they also result in long range structures with characteristic shapes [4] and spacings [5]. In general, the surfaces used in these investigations are grown by molecular beam epitaxy or chemical vapor deposition where the system is far from equilibrium both in terms of the flux of impinging molecules and the chemical potential. In this regime, growth progresses either by step flow at preexisting steps on vicinal surfaces or through layer-by-layer and multilayer growth on nucleating islands [4,6]. A few studies [7,8] have used atomic force microscopy (AFM) to investigate the advance of inorganic, single crystal surfaces grown at low supersaturation where the classic dislocation controlled mode of growth first described by Burton, Cabrera, and Frank (BCF) [9] should be applicable. The results of these studies show that while the growth rate may be controlled by kinetic factors such as diffusion or monomer incorporation, the morphology itself generally conforms to the BCF picture. To date, little is known about the differences or similarities between these growth modes and those of macromolecular crystals.

The use of macromolecular systems for the investigation of crystal growth provides a distinct advantage over that of most inorganic systems: Slow growth kinetics [10] and large molecular diameters make macromolecular crystals ideal systems for the real time AFM investigations of growth. The limitations due to the rapid kinetics of atomic motion and the influences of the voltage at the tip on that motion that are encountered in real time scanning tunnel microscope (STM) investigations of semiconductors [11,12] and metals [13] are avoided. Following the demonstration of AFM as a useful tool for investigating both *in situ* crystal growth [7] and biological structures [14], Durbin and Carlson [15] successfully used AFM to monitor the solution growth of single crystals of the protein lysozyme. Their observations, though limited, were at least consistent with the general physical picture of growth first developed for inorganic systems by Burton, Cabrera, and Frank [9]: Growth occurred both by step flow on steps generated by screw dislocations and by 2D nucleation.

Because of their large size ($\geq$17 nm), spherical shapes, and simple packing geometries, icosahedral viruses provide especially good models for investigation of macromolecular crystallization. We have chosen to investigate the $T = 1$ satellite tobacco mosaic virus (STMV) because its structure has been accurately determined, it is easily and reproducibly crystallized under a wide range of conditions, and it has been well studied using other techniques. Previously, the aggregation pathway leading to the formation of 3D critical nuclei of STMV was analyzed by quasielastic light scattering (QELS) [16], and crystallization kinetics were investigated by Michelson interferometry [10]. Yet, little is known about the actual growth mechanisms and molecular scale processes. The purpose of this Letter is to report the results of the first nanometer scale study of virus crystallization using *in situ* AFM. The actual growth mechanisms and the fundamental parameters that characterize the growth process are determined from the images. Our results show that growth of

 0031-9007/95/75(14)/2778(4)$06.00

STMV occurs through the nucleation of 2D islands and layer-by-layer advancement of 14 ± 0.9 nm monomolecular steps. New islands nucleate on the terraces of adsorbed 3D nuclei, then continue to grow and coalesce resulting in step bunching and formation of "stacks" consisting of 10–20 monolayers. The size of small islands that continued to grow as well as small islands that dissolved provide an estimate of the critical radius size. From the size of the critical radius, the free energy of the step edge α is determined, and from the speed of the steps the kinetic coefficient for step motion β is calculated.

The STMV used in this study was purified using rate zone density-gradient centrifugation from coinfected tobacco mosaic virus U5-infected leaves from six-week-old tobacco plants infected in the third week. This is the smallest virus yet obtained in crystalline form, having a diameter of ~16 nm and a molecular weight of 1.45×10^6 Da. This study is focused on the development of the (111) face of cubic STMV crystals. The crystals were grown on etched silica substrates over a period of days by incubation of 2.3 mg/ml STMV solution with an equal volume of 40% saturated ammonium sulfate in the fluid cell of the commercial Nanoscope III AFM [7] under conditions of no flow. The final crystal sizes were in the range of 30–50 μm. Images were collected in contact mode using cantilevers with nominal force constants of 0.06 to 0.38 $N m^{-1}$. Forces of <0.1 to 0.5 nN were applied during imaging.

Presented in Fig. 1 is a 1×1 μm AFM image of the (111) plane of a cubic crystal of STMV where the individual virus monomers, with center-to-center distances of 18 nm, are clearly resolved. The lower portion of the image has been Fourier filtered for clarity. The structure of the orthorhombic form of STMV has been solved [17], and that of the cubic crystal form was determined by x-ray diffraction experiments to have space group P23 with unit cell parameters of $a = b = c = 25.7$ nm [18]. However, the packing and the exact centers of the virus particles in the unit cell were unknown. The hexagonal array of the (111) plane and the intermolecular spacings determined from the images show that the molecules have face centered cubic (fcc) packing. This could not be determined from the x-ray data because the STMV molecule itself does not possess the fourfold symmetry of the fcc lattice.

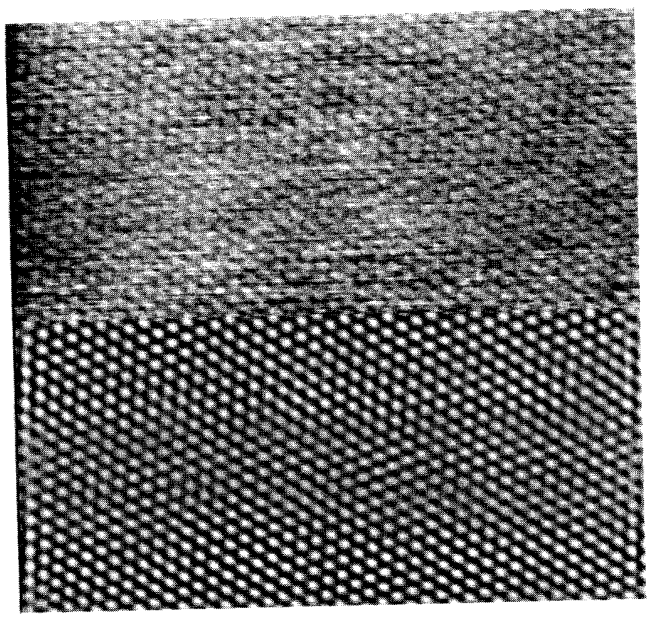

FIG. 1. 1×1 μm AFM image of the (111) plane of a cubic crystal of STMV. The lower portion of the image has been Fourier filtered. The hexagonal array showing individual virus particles, with center-to-center distances of 18 nm, is clearly seen.

The growth of STMV was observed to occur by 2D and 3D nucleation to form "stacks" of 10 to 20 monolayers followed by layer-by-layer advancement of the 14 nm monomolecular steps. Surprisingly, no dislocations were observed on STMV crystals in numerous experiments. The stacks served as the growth centers for the crystals. Stack formation was initiated by 3D nucleation and by adsorption of microcrystals from solution with the proper orientation for growth. This formation process was observed repeatedly. The growth of one of these stacks is shown in Fig. 2. The 7.5×7.5 μm image in Fig. 2(a) shows the stack shortly after it was formed. Figures 2(b)–2(d) are 25×25 μm images taken at successively later times. In these images, the stack has grown to ~23 μm in diameter. New islands are observed to nucleate on the larger terraces. These islands then continue to grow and coalesce with other islands on the same ter-

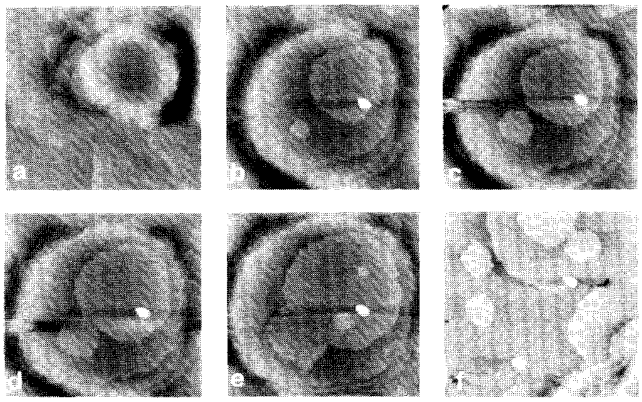

FIG. 2. Series of AFM images showing nucleation, growth, and coalescence of islands and expansion of a "stack." (a) 7.5×7.5 μm image of the stack in its early stages ($t = 0$). Note that the micron sized particle seen in images (b)–(f) is not present here. (b)–(e) 25×25 μm images showing 2D nucleation, coalescence, and growth of the stack ($t = 1500$, 1590, 1670, and 1840 sec). (f) 23×23 μm image taken at a later time ($t = 3520$ sec). The approach of another stack can be seen in the lower right portion of the image.

race. Growth continues radially outward with eventual step bunching at the edges of the stacks.

For growth to occur by 2D nucleation a stable nucleus with a radius $r > r_c$ must first be formed. A critical nucleus represents a local free energy maximum where for $r < r_c$ dissolution occurs, while for $r > r_c$ growth proceeds, in both cases with a decrease in free energy. In our experiments we observed small stable islands that continued to grow as well as small islands that dissolved. Measurements of these islands provide a bracket for the size of the critical nucleus necessary for growth to occur. As illustrated in Fig. 3, islands with radii greater than 200 nm continued to develop while those with radii less than 100–200 nm consistently dissolved, constraining r_c to be in the range of 100–200 nm. The size [9,19] of the critical radius is related to the free energy of the step edge α by

$$r_c = \omega\alpha/kT\sigma,$$

where $\omega = 4.2 \times 10^{-18}$ cm^{-3} is the specific volume of an STMV monomer in the crystal, k is Boltzmann's constant, $\sigma = \ln(c/c_e) = 1.8$ is the solution supersaturation, and T is the temperature. From this relationship we estimate the value of the free energy to be $(2.6 \pm 0.9) \times 10^{-1}$ erg/cm^2. The corresponding free energy per virus particle with a surface area s satisfies the relationship $\alpha s/kT \gg 1$ indicating that the faces of STMV crystals should be atomically smooth and develop by step motion [9,19] as is observed here.

The value of α determined in these experiments is similar to the value obtained for the protein canavalin [20] and is consistent with those previously estimated by QELS [16] (although the value of α determined from a 3D nucleus is not necessarily the same as the value obtained from a 2D nucleus). The value obtained for α is 1 to 2 orders of magnitude lower than for conventional inorganic crystals grown from solution [21]. The low value probably reflects the high solvent content (30%–90%) of macromolecular crystals [22] since the near equivalence of environments in solution and in the crystal should lower the amount of work required to create a surface unit of the crystal. The low value for α is also a consequence of the scarcity and marginal strength of intermolecular interactions per lattice unit in macromolecular crystals.

Another important growth parameter is the kinetic coefficient β, which relates the speed of an elementary step to the supersaturation through the relationship [9,19]

$$v = \omega\beta(c - c_e),$$

where $c = 3.4 \times 10^{14}$ cm^3 and $c_e = 5.6 \times 10^{13}$ cm^3 are the initial and equilibrium volume concentrations of the dissolved STMV in solution. The kinetic coefficient itself is a measure of the kinetics of adsorption, diffusion, and incorporation with the rate limiting step dominating the value of β. From the experimental rates of step advancement, $v = (5–10) \times 10^{-7}$ cm/sec, we estimate β to be $(6 \pm 2) \times 10^{-4}$ cm/sec for STMV. This value is similar to that found for canavalin protein crystals [20]. The kinetic coefficient for biological macromolecules is 2 or 3 orders of magnitude lower than for inorganic crystals grown from solution [23]. This low value of β indicates that the low growth rates of macromolecular crystals in comparison with inorganic crystals must be due to a greatly lowered overall probability of incorporation of individual molecules into the growing crystal. Explanations for the low values of β for macromolecular systems include a potentially large barrier to adsorption (shedding the hydration layer), a low surface diffusivity, and a low probability of the molecule having the proper molecular orientation for direct incorporation into the crystal.

Information about factors that limit growth is also obtained from these images. As seen in Fig. 2, newly formed islands expand and eventually reach the edge of the preceding terrace, resulting in step bunching and formation of a stack. The speed of newly formed islands and that of macro steps (bunched step trains of stacks) differ by less than 25%. While this difference is enough to cause the steps to bunch, the similar values for the mono and macro step rates imply that no significant overlap of the diffusion fields exists. The images shown in Figs. 2 and 3 show the step train from another stack traversing the surface from the lower right side. This has important implications as it demonstrates that, unlike the case of canavalin [20] and calcite [24] growth, the

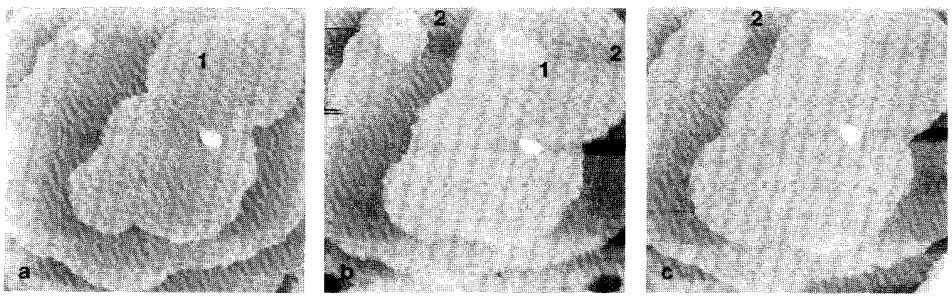

FIG. 3. This sequence is 23 × 23 μm AFM images, taken at 86 sec intervals, showing two-dimensional nuclei forming on a surface. A two-dimensional hypercritical nucleus of radius 315 nm continues to grow [labeled **1** in (a) and (b)], while a subcritical two-dimensional nucleus with radius of 165 nm dissolves [labeled **2** in (b) and (c)].

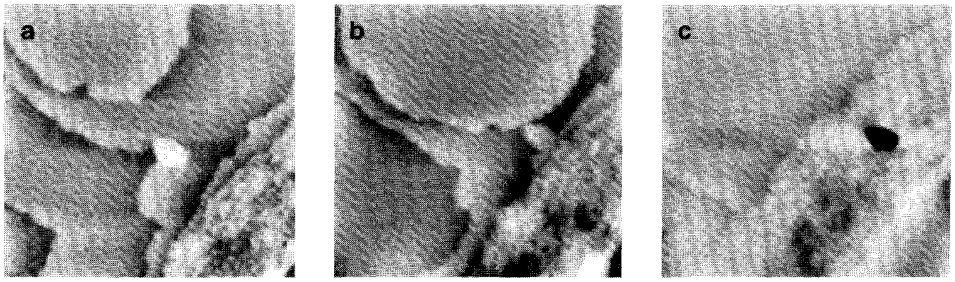

FIG. 4. Sequence of 12 × 12 mm AFM images showing the incorporation of a micron sized particle where (a) the particle is several layers above the surface (t = 5140 sec), (b) the layers have accumulated around it so that it extends about one monolayer above the surface (t = 5440 sec), and (c) the particle has been incorporated into the growing crystal leaving a micron sized channel in the crystal (t = 5860 sec).

mixing of the solution caused by scanning does not result in enhanced growth relative to the rest of the crystal, suggesting that growth is not bulk diffusion limited. Thus, we suggest that cubic STMV crystal growth is limited by the kinetics of monomer incorporation, rather than by surface or volume diffusion.

A recurring question in macromolecular crystal growth is the nature and influence of incorporated impurities and the degree to which they affect the properties of crystals. Numerous observations of impurity effects were made in this AFM study. One interesting example was the observation of a micron sized particle that sedimented on the crystal surface during the experiment. In Fig. 2(a) the beginning of the stack is shown with no particle present. In all subsequent images, Figs. 2(b)–2(f), 3, and 4, a micron sized particle is present on the surface. Figure 4 illustrates the process of particle incorporation and defect formation similar to that observed by Durbin [15]. Initially, the particle is projected above the surface as seen in Fig. 4(a). In Fig. 4(b) the particle is just one layer above the surface and the step is beginning to enclose it. As Fig. 4(c) shows, subsequent steps close around the former site of the particle, leaving a persistent micron sized channel in the crystal [see Fig. 4(c)].

This work was performed under the auspices of the Division of Materials Science, U.S. Department of Energy and Lawrence Livermore National Laboratory, and was supported by grants from NASA. We thank S. B. Larson for his assistance.

[1] A. McPherson, Sci. Am. **260**, No. 3, 62 (1989).
[2] C. Branden and J. Tooze, *Introduction to Protein Science* (Garland Publishing Inc., New York, 1991).
[3] Y. W. Mo, J. Kleiner, M. B. Webb, and M. G. Lagally, Phys. Rev. Lett. **66**, 1998 (1991); Surf. Sci. **268**, 275 (1992).
[4] M. D. Johnson, C. Orme, A. W. Hunt, D. Graff, J. Sudijono, L. M. Sander, and B. G. Orr, Phys. Rev. Lett. **72**, 116 (1994).
[5] J. E. Van Nostrand, S. J. Chey, M. A. Hasan, D. G. Cahill, and J. E. Greene, Phys. Rev. Lett. **74**, 1127 (1995).
[6] J. Tersoff, A. W. Denier van der Gon, and R. M. Tromp, Phys. Rev. Lett. **72**, 266 (1994).
[7] A. J. Gratz, S. Manne, and P. K. Hansma, Science **251**, 1343 (1991).
[8] J. J. De Yoreo, T. A. Land, and B. J. Dair, Phys. Rev. Lett. **73**, 838 (1994).
[9] W. K. Burton, N. Cabrera, and F. C. Frank, Philos. Trans. R. Soc. London, Ser. A **243**, 299 (1951).
[10] Yu. G. Kuznetsov, A. J. Malkin, A. Greenwood, and A. McPherson, J. Struct. Biol. **114**, 184 (1995).
[11] N. Kitamura, M. G. Lagally, and M. B. Webb, Phys. Rev. Lett. **71**, 2082 (1993).
[12] E. Ganz, S. K. Theiss, I-S. Hwang, and J. Golovchenko, Phys. Rev. Lett. **68**, 1567 (1992).
[13] S. J. Stranick, M. M. Kamna, and P. S. Weiss, Science **266**, 99 (1994).
[14] P. K. Hansma, V. B. Elings, O. Marti, and C. E. Bracker, Science **242**, 209 (1988).
[15] S. D. Durbin and W. E. Carlson, J. Cryst. Growth **122**, 71 (1992); see also S. D. Durbin, J. Phys. D **26**, B128 (1993).
[16] A. J. Malkin and A. McPherson, Acta Crystallogr. Sect. D **50**, 385–395 (1994).
[17] S. B. Larson, S. Koszelak, J. Day, A. Greenwood, J. A. Dodds, and A. McPherson, Nature (London) **361**, 179–182 (1993).
[18] S. Koszelak, J. Day, C. Lega, R. R. Cudney, and A. McPherson, Biophys. J. **69**, 13 (1995).
[19] A. A. Chernov, in *Modern Crystallography III. Crystal Growth* (Springer, Berlin and New York, 1984), Vol. 36.
[20] T. A. Land, A. J. Malkin, Yu. G. Kuznetsov, A. McPherson, and J. J. DeYoreo, Phys. Rev. Lett. **75**, 2774 (1995).
[21] O. Sôhnel, J. Cryst. Growth **57**, 101–108 (1982).
[22] G. L. Gilliland, M. Tung, D. M. Blakeslee, and J. E. Ladner, Acta Crystallogr. Sect. D **50**, 408–413 (1994).
[23] A. A. Chernov, L. N. Rashkovich, I. Smol'skii, Yu. G. Kuznetsov, A. A. Mkrtchyan, and A. J. Malkin, in *Growth of Crystals* (Consultants Bureau, New York, 1988), Vol. 15, pp. 43–92.
[24] A. J. Gratz, P. E. Hilner, and P. K. Hansma, Geochim. Cosmochim. Acta **57**, 491 (1993).

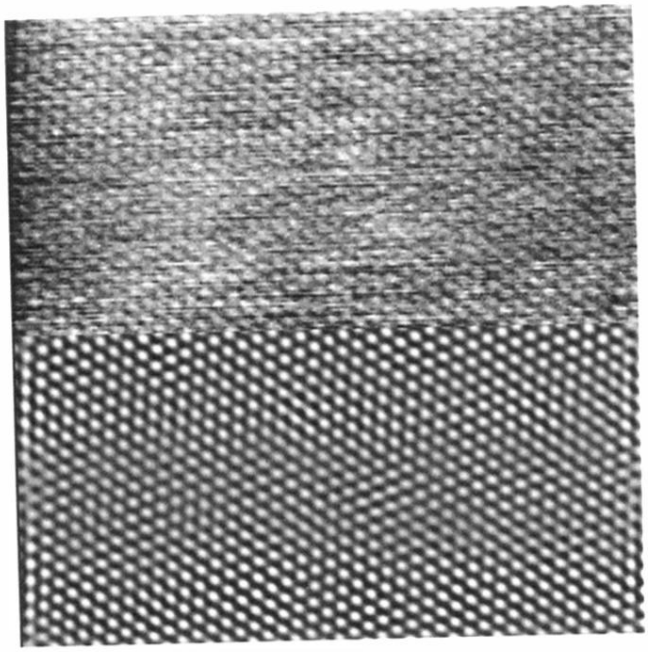

FIG. 1. 1×1 μm AFM image of the (111) plane of a cubic crystal of STMV. The lower portion of the image has been Fourier filtered. The hexagonal array showing individual virus particles, with center-to-center distances of 18 nm, is clearly seen.

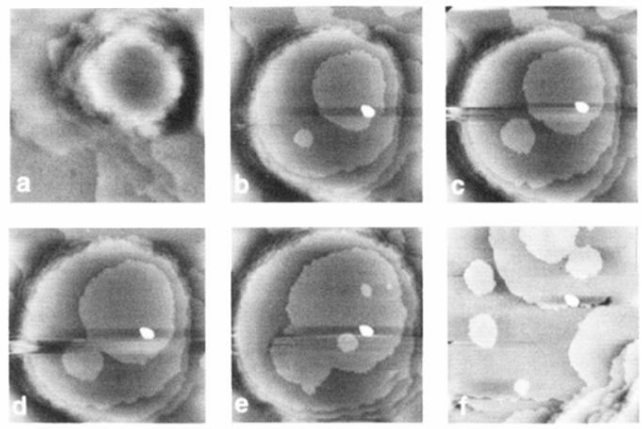

FIG. 2. Series of AFM images showing nucleation, growth, and coalescence of islands and expansion of a "stack." (a) 7.5×7.5 μm image of the stack in its early stages ($t = 0$). Note that the micron sized particle seen in images (b)–(f) is not present here. (b)–(e) 25×25 μm images showing 2D nucleation, coalescence, and growth of the stack ($t = 1500$, 1590, 1670, and 1840 sec). (f) 23×23 μm image taken at a later time ($t = 3520$ sec). The approach of another stack can be seen in the lower right portion of the image.

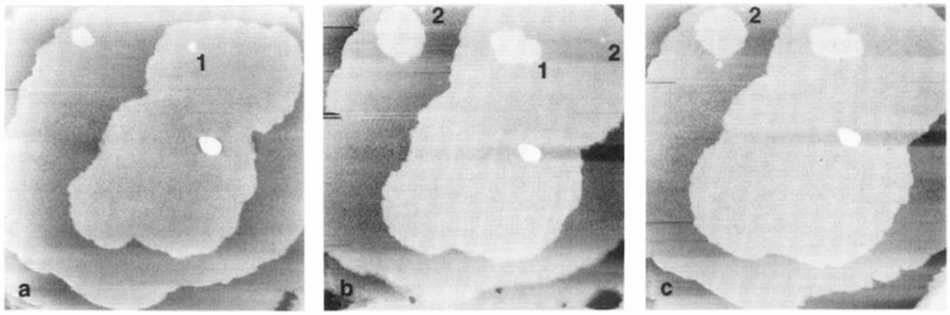

FIG. 3. This sequence is 23 × 23 μm AFM images, taken at 86 sec intervals, showing two-dimensional nuclei forming on a surface. A two-dimensional hypercritical nucleus of radius 315 nm continues to grow [labeled **1** in (a) and (b)], while a subcritical two-dimensional nucleus with radius of 165 nm dissolves [labeled **2** in (b) and (c)].

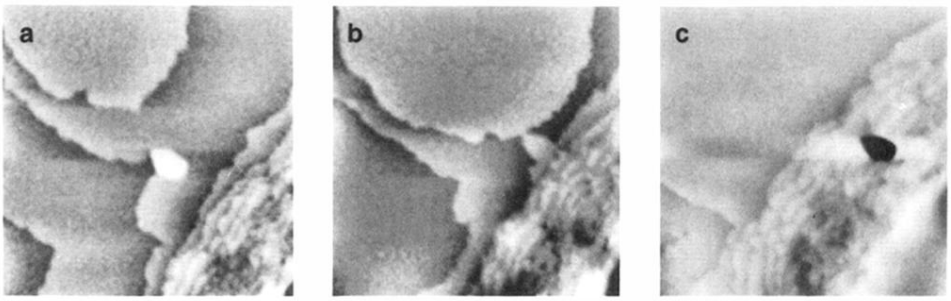

FIG. 4. Sequence of 12 × 12 mm AFM images showing the incorporation of a micron sized particle where (a) the particle is several layers above the surface ($t = 5140$ sec), (b) the layers have accumulated around it so that it extends about one monolayer above the surface ($t = 5440$ sec), and (c) the particle has been incorporated into the growing crystal leaving a micron sized channel in the crystal ($t = 5860$ sec).